ROYAL SOCIETY OF CHEMISTRY

PAPER

Check for updates

Unravelling the structure–luminescence relationship in two dimensional antimony(III)-doped cadmium(II) halide hybrids†

Ashwath Kudlu,‡[a] Dhritismita Sarma,‡[b] Deep Kumar Das,[a] Alisha Basheer Shamla,[a] Rangarajan Bakthavatsalam, [c] Venkatesha R. Hathwar,[d] Arup Mahata*[b] and Janardan Kundu *[a]

Luminescent zero dimensional (0D) antimony halide (Sb–X) hybrids showcase emissive properties (emission peak position; photoluminescence quantum yield – PLQY) that are strongly dependent on the local metal halide geometry/site asymmetry. However, controlling the local metal halide geometry has been synthetically challenging due to the diverse coordination geometries adopted by the Sb–X units. Consequently, efforts ascertaining a clear structure–luminescence relation in 0D Sb–X hybrids have met with limited success. Reported here is an attempt to draw a structure–luminescence relationship by controlling the Sb–X geometry utilizing 2D cadmium halide hybrids as the host that serves as a framework for incorporating emissive Sb^{3+} dopants. The choice of a series of organic cations tunes the local metal halide geometry/distortion in the host hybrids that controllably alters the luminescent properties of the emissive dopants in 2D Sb^{3+} doped hybrids. A clear structure–luminescence relationship is observed: red-shifted emission peak positions and enhanced PLQYs as the extent of the local metal halide distortion increases. DFT calculations of the doped compounds, characterizing ground and excited state structural and electronic properties, reveal the operative luminescence mechanism and the origin of different efficiency of luminescence (PLQY). This work provides deeper insight into the luminescence mechanism highlighting the importance of ground and excited state structural distortions in Sb^{3+} doped 2D cadmium halide hybrids. The experimental–computational insights gained here are beneficial for establishing the structure–luminescence relationship for 0D Sb halide hybrids targeting their rational synthesis.

Introduction

Luminescent low dimensional (2D, 1D, 0D) metal halide hybrids have emerged as a paradigm-changing class of functional materials appropriate for applications in solid state lighting.[1–19] Derived from the ABX_3 perovskite structure, the lower dimensional hybrid variants, incorporating organic cations and halometallate units, enjoy huge chemical phase space flexibility with varied networking/connectivity of the metal halide units.[9,16] 2D hybrids with alternating planes of corner shared metal halide units and organic cations crystallize in the Ruddlesden–Popper (RP) or Dion–Jacobson (DJ) phase (guided by the nature of the organic cation), and have bound excitons delocalized over the inorganic plane.[1,11–15,18,19] On the other hand, 0D hybrids with isolated metal halide units dispersed in the matrix of the organic cations have a unique electronic structure supporting highly confined excitons within the metal halide units appropriate for radiative recombination/lighting applications.[2,3,7,9,20–26] Numerous efforts have been reported utilizing various types of metal halide units (M = Sb, Mn, Te, In, Cd; X = Cl, Br, I) with different kinds of organic cations (ammonium, phosphonium, alkyl, aryl) for the synthesis and photo-physical property analysis of 0D metal halide hybrids.[2–6] Among them, Sb^{3+} based 0D metal halide hybrids appear at the research forefront due to their strong luminescence and rich coordination chemistry of the Sb–halide units crystallizing in various geometries (octahedral, square pyramidal, trigonal pyramidal, disphenoidal, *etc.*).[20–22,26–30] Local metal halide

a Indian Institute of Science Education and Research (IISER) Tirupati, Tirupati, Andhra Pradesh 517507, India. E-mail: janardan@iisertirupati.ac.in

b Indian Institute of Technology Hyderabad Sangareddy, Kandi, Telangana 502284, India. E-mail: arup@chy.iith.ac.in

c B.M.S College of Engineering, Bull Temple Road, Bengaluru, Karnataka 560019, India

d School of Physical and Applied Sciences, Goa University, Panaji, Goa 403206, India

geometry dependent photo-physical properties (photoluminescence emission peak – PL peak; photoluminescence quantum yield – PLQY) of 0D Sb halide hybrids have thus been reported with PL peaks spanning the visible range with low to high values of PLQY.[22,26,27,29,30] Landing on a rational design strategy to target photo-physical properties of 0D Sb halide hybrids necessitates unravelling the operative structure–luminescence relation. Consequently, synthetic efforts have been devoted to rationalizing their emissive properties but the structure–luminescence correlation in such 0D Sb–halide hybrids is still unclear.[22,26,27,30] This absence of the structure–luminescence correlation is primarily due to the diverse coordination geometries adopted by Sb–halide units wherein controlling the local metal halide geometry has proven to be synthetically challenging.

In order to reliably control the Sb halide geometry/asymmetry and unravel the operative structure–luminescence correlation, a synthetic strategy of Sb^{3+} doping[31–36] into 2D metal halide host hybrids incorporating different organic ammonium cations is exploited here. High band gap 2D octahedral cadmium chloride host hybrids, having different Cd–halide local geometry/site asymmetry, undergo heterovalent substitutional doping with Sb^{3+} dopant ions (Sb^{3+} ionic radii $\sim$ 0.76 Å; Cd^{2+} ionic radii $\sim$ 0.95 Å)[37] allowing control over the local metal halide geometry around the dopant centre. Here, Sb^{3+}-doped 2D octahedral cadmium halide hybrids with different metal halide geometry/site asymmetry mimic the 0D Sb halide hybrids with different site symmetry and provide a systematic route to correlate their structure with their photo-physical properties. Specifically, a series of Sb^{3+} doped octahedral cadmium chloride 2D DJ hybrids have been crystallized utilizing different organic amines [1,5-diaminopentane (denoted as PDA); 1,4-diaminobutane (denoted as DAB); and diethylenetriamine (denoted as DETA); Scheme 1], which allows controlled tuning of the local metal halide octahedral geometry (around metal/Sb^{3+} dopant center). Single crystal structural analysis (SCXRD) of the compounds reveals that the synthesized 2D doped hybrids have emissive Sb^{3+} dopants with octahedral metal chloride geometry showcasing different extents of distortions/site asymmetry as quantitated by the distortion indices (bond length distortion, bond angle variance). Correlated with such differences in the ground state distortions, PL peak positions of the compounds are observed to redshift from 520 nm to 560 nm as the extent of distortion increases. Concomitantly,

these compounds show extreme values of PLQY (ranging from 60% to $\sim$96%) with the observed strong correlation of higher PLQY for compounds manifesting higher structural distortion. Such differences in the photo-physical properties of the compounds, bearing correlation with ground and excited state energetic and electronic behavior, reveals the origin of the extent of better luminescence in the Sb-doped structures. Through systematic synthetic efforts and DFT calculations, this work successfully unravels the underlying structure–luminescence relationship in 2D Sb^{3+}-doped cadmium halide hybrids that provides deeper insight into the observed photo-physical properties (PL peak position; PLQYs) highlighting the importance of ground and excited state structural distortions. Such insight is beneficial for establishing the structure–luminescence relationship for luminescent 0D Sb halide hybrids enabling their rational design and targeted synthesis for lighting applications.

Experimental section

Materials

Cadmium chloride hemi(pentahydrate) (ACS reagent, 79.5–81%), antimony(III) oxide (99%), hydrochloric acid (37%) and acetone were purchased from Sigma Aldrich. Diethylenetriamine ($>$98.0% (GC)), 1,5-diaminopentane ($>$98.0%) and 1,4-diaminobutane ($>$98.0% (GC)) were purchased from TCI Chemicals. All chemicals were used without further purification.

Synthesis of DETACdCl

Single crystals of cadmium(II) halide hybrids with a DETA ligand (DETACdCl) were synthesized by dissolving 1 mmol of $CdCl_2$ (228.36 mg) in 12 mL of HCl through sonication at room temperature. After getting a clear solution, 1 mmol of diethylenetriamine (103.17 mg) was added in an ice bath with constant stirring. The mixture was heated to 100 °C until a clear solution was obtained. The resultant solution was slowly cooled to room temperature. Colorless crystals were obtained within a day. The crystals were filtered, washed with acetone and dried in a vacuum oven at 60 °C overnight.

Synthesis of x% Sb:DETACdCl (x = 5, 10, 20, 30, 40, 50)

Single crystals of antimony(III)-doped cadmium(II) halide hybrids with a DETA ligand (x%Sb:DETACdCl) were synthesized by dissolving $CdCl_2$ (1 − x mmol) and 0.5x mmol of Sb_2O_3 (x = 0.05, 0.1, 0.2, 0.3, 0.4, 0.5) in 12 ml of HCl through sonication at room temperature. To the resultant clear solution, 1 mmol of diethylenetriamine (103.17 mg) was added in an ice bath with constant stirring. The mixture was heated to 100 °C until a clear solution was obtained. The resultant solution was slowly cooled to room temperature. Colorless crystals were obtained, which emit green in UV light. The crystals were filtered, washed with acetone and dried in a vacuum oven at 60 °C overnight.

Synthesis of DETASbCl

Single crystals of antimony(III) halide hybrids with DETA ligand DETASbCl were synthesized by dissolving 0.5 mmol of Sb_2O_3
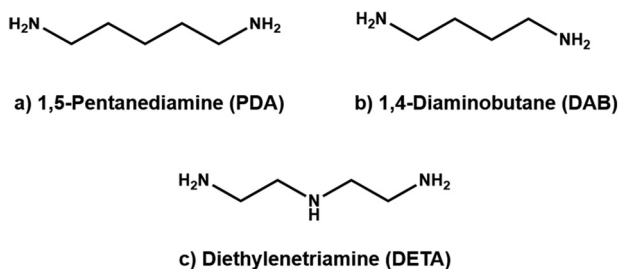
Scheme 1 Different organic amines (and their acronym) utilized for the synthesis of various 2D host (undoped), Sb(III) doped Cd(II) halide hybrids, and control hybrids: (a) 1,5-pentanediammonium; (b) 1,4-diammoniumbutane; (c) diethylenetriamine.

(145.76 mg) in 7 ml of HCl through sonication at room temperature. After getting a clear solution, 1 mmol of diethylenetriamine (103.17 mg) was added in an ice bath with constant stirring. The mixture was heated to 100 °C until a clear solution was obtained. The resultant solution was slowly cooled to room temperature. Colorless crystals were obtained within a day. The crystals were filtered, washed with acetone and dried in a vacuum oven at 60 °C overnight.

Synthesis of PDACdCl

Single crystals of cadmium(II) halide hybrids with a PDA ligand (PDACdCl) were synthesized by dissolving 1 mmol of $CdCl_2$ (228.36 mg) in 10 ml of HCl through sonication at room temperature. After getting a clear solution, 1 mmol of diaminopentane (102.18 mg) was added in an ice bath with constant stirring. The mixture was heated to 100 °C until a clear solution was obtained. The resultant solution was slowly cooled to room temperature. Colorless crystals were obtained after one day. The crystals were filtered, washed with acetone and dried in a vacuum oven at 60 °C overnight.

Synthesis of x% Sb:PDACdCl (x = 5, 10, 20, 30, 40, 50)

Single crystals of antimony(III)-doped cadmium(II) halide hybrids with PDA ligand (x%Sb:PDACdCl) were synthesized by dissolving $CdCl_2$ (1 − x mmol) and 0.5x mmol of Sb_2O_3 (x = 0.05, 0.1, 0.2, 0.3, 0.4, 0.5) in 10 ml of HCl through sonication at room temperature. To the resultant clear solution, 1 mmol of diaminopentane (102.18 mg) was added in an ice bath with constant stirring. The mixture was heated to 100 °C until a clear solution was obtained. The resultant solution was slowly cooled to room temperature. Colorless crystals were obtained, which emit weak yellow in UV light. The crystals were filtered, washed with acetone and dried in a vacuum oven at 60 °C overnight.

Synthesis of PDASbCl

Single crystal antimony(III) halide hybrids with the PDA ligand (PDASbCl) were synthesized by dissolving 0.5 mmol of Sb_2O_3 (145.76 mg) in 7 ml of HCl through sonication at room temperature. After getting a clear solution, 1 mmol of diaminopentane (102.18 mg) was added in an ice bath with constant stirring. The mixture was heated to 100 °C until a clear solution was obtained. The resultant solution was slowly cooled to room temperature. Colorless crystals were obtained after three days. The crystals were filtered, washed with acetone and dried in a vacuum oven at 60 °C overnight.

Synthesis of DABCdCl

Single crystals of cadmium(II) halide hybrid with DAB ligand (DABCdCl) were synthesized by dissolving 1 mmol of $CdCl_2$ (228.36 mg) in 10 ml of HCl through sonication at room temperature. After getting a clear solution, 1 mmol of diamino butane (88.15 mg) was added in an ice bath with constant stirring. The mixture was heated to 100 °C until a clear solution was obtained. The resultant solution was slowly cooled to room temperature. Colorless crystals were obtained after one day. The crystals were filtered, washed with acetone and dried in a vacuum oven at 60 °C overnight.

Synthesis of x% Sb:DABCdCl (x = 5, 10, 20, 30, 40, 50)

Single crystals of antimony(III) doped cadmium(II) halide hybrid with a DAB ligand (x%Sb:PDACdCl) were synthesized by dissolving $CdCl_2$ (1 − x mmol) and 0.5x mmol of Sb_2O_3 (x = 0.05, 0.1, 0.2, 0.3, 0.4, 0.5) in 10 ml of HCl through sonication at room temperature. To the resultant clear solution, 1 mmol of diamino butane (88.15 mg) was added in an ice bath with constant stirring. The mixture was heated to 100 °C until a clear solution was obtained. The resultant solution was slowly cooled to room temperature. Colorless crystals were obtained, which emit weak orange in UV light. The crystals were filtered, washed with acetone and dried in a vacuum oven at 60 °C overnight.

Dehydrated Sb:DABSbCl hybrid was obtained by heating the freshly synthesized Sb:DABCdCl hybrid in a 100 ml Schlenk flask to remove the water. The dehydration at 150 °C for three hours is done using a Schlenk line with continuous vacuum of the argon gas environment in the flask. It is then allowed to cool down to room temperature naturally in an argon environment and stored in a glovebox for further analysis.

Synthesis of DABSbCl

Single crystals of antimony(III) halide hybrid with DAB ligand (DABSbCl) were synthesized by dissolving 0.5 mmol of Sb_2O_3 (145.76 mg) in 7 ml of HCl through sonication at room temperature. After getting a clear solution, 1 mmol of diamino butane (88.15 mg) was added in an ice bath with constant stirring. The mixture was heated to 100 °C until a clear solution was obtained. The resultant solution was slowly cooled to room temperature. Colorless crystals were obtained after three days. The crystals were filtered, washed with acetone and dried in a vacuum oven at 60 °C overnight.

Methods

Solid-state UV-vis absorption measurements were carried out in an Agilent Cary Series UV-vis-NIR spectrophotometer with an integrating sphere accessory. Steady state PL and PLE were measured using a JASCO FP-8500 spectrofluorometer. The low temperature PL and PLE, lifetime and absolute quantum yield were recorded on an Edinburgh FLS 1000 photoluminescence spectrometer with an Optistat DN cryostat. The temperature was controlled by a Mercury ITC temperature controller (Oxford Instruments). Powder X-ray diffraction of the samples was recorded on a Rigaku SmartLab with a Cu Kα source (λ = 1.5406 Å). Samples for powder X-ray diffraction were prepared by mechanical grinding of single crystals. Single-crystal X-ray diffraction data for the crystals were collected on a Bruker APEX II single-crystal X-ray CCD diffractometer having graphite monochromatized (Mo Kα, λ = 0.71073 Å) radiation at 100.0 K. Data reduction was performed using APEX II software. Intensities for absorption were corrected with SADABS, and using Olex2, the structure was solved with the SHELXS structure solution program using direct methods and refined with the SHELXL refinement package using least-squares minimization, with anisotropic displacement parameters for all non-H atoms. Technical details of data acquisition, selected crystal refinement results, and selected bond distances and angles are reported in the ESI.† Mercury software was used to prepare ORTEPs and packing diagrams.

810 | J. Mater. Chem. C, 2025, 13, 808–820

This journal is © The Royal Society of Chemistry 2025

Computational details

The first-principles calculations based on density functional theory (DFT) were carried out within the PWSCF Quantum-Espresso package.[38] Geometry optimization employs the GGA-PBE level of theory, with the consideration of dispersion correction with DFT-D3[39] while ultrasoft pseudo-potentials are used to describe electron–ion interactions, with explicit inclusion of atomic orbitals from Cd (5s, 5p, 4d), Sb (5s, 5p, 4d), Cl (3s, 3p), N and C (2s, 2p), and H (1s).[40] The plane-wave basis set is employed with cutoffs of 25 Rydbergs for the smooth part of the wave functions and 200 Rydbergs for the augmented density. Electronic structure calculations were performed using the Heyd Scuseria Ernzerhof (HSE06) functional[41] with 25% Hartree–Fock (HF) exchange, including spin orbit coupling (SOC). The norm-conserving basis set is employed with cutoffs of 40 Rydbergs for the smooth part of the wave functions and 80 Rydbergs for the augmented density. The band structures are also calculated along high-symmetry k points using the PBE + SOC approach. The excited state geometry optimization has been performed using the CP2K software package[42] using the PBE0 hybrid exchange–correlation functional with 25% HF exchange, including van der Waals interactions with the DFT-D3 scheme. The auxiliary density matrix method with the cFIT auxiliary basis set was applied to accelerate the optimization of ionic positions within the hybrid functional calculations.[43] The electron–hole overlap percentages were calculated by the volume normalised ratio of the overlapped charge density between the electron and hole to the total charge density of both the electron and hole.

Results and discussion

Synthesis of the undoped cadmium halide hybrid host, control hybrids, and Sb-doped cadmium halide hybrids involved dissolving the desired organic amine (Scheme 1) and requisite metal halide precursors in HCl at ~100 °C, followed by cooling to room temperature to yield single crystals. Varying levels of Sb^{3+} doping in host hybrids were achieved by utilizing the requisite amount of Cd and Sb precursor during the synthesis. A detailed description of the synthetic procedure followed is provided in the experimental section. As depicted in Scheme 1, different organic amines—1,5-diaminopentane (denoted as PDA), 1,4-diaminobutane (denoted as DAB), and diethylenetriamine (denoted as DETA)—were chosen as organic cation precursors for the synthesis of Sb-doped cadmium chloride hybrids to strongly influence the local metal halide geometry/structure. The presence of cadmium (Cd), antimony (Sb), and chlorine (Cl) in the resulting crystals was confirmed through SEM-EDS and ICP analysis as shown in Fig. S1–S3, and Table S1, ESI.† For brevity and convenience, the Sb-doped cadmium chloride hybrid synthesized using 1,5-diaminopentane is denoted as Sb:PDACdCl, and the corresponding undoped host sample is denoted as PDACdCl, while the control system is denoted as PDASbCl. Similar denotation of samples is followed for the utilized organic amines here for convenience.

Single-crystal X-ray diffraction (ScXRD) analysis revealed that the prepared compounds (host and doped hybrids) crystallize in a Dion–Jacobson (DJ)-type corner shared 2D structure with alternating metal halide and organic layers. Fig. 1(a)–(c) shows the asymmetric unit and crystal packing diagram of the Sb-doped cadmium chloride hybrids. The anionic $[(Cd/Sb)Cl_6]^{2-}$ octahedral units are charge balanced by the chosen protonated organic cations. As evident from the ICP data (Table S1; ESI†), Sb^{3+} ions (ionic radius ~ 0.76 Å) undergo substitutional doping at the Cd^{2+} sites (ionic radius ~ 0.95 Å) of the host 2D framework in low amounts due to the differences in their ionic sizes.[37] The crystal structure of the doped hybrid halides is found to be similar to that of the corresponding host structure (Fig. S4; ESI†). The ScXRD
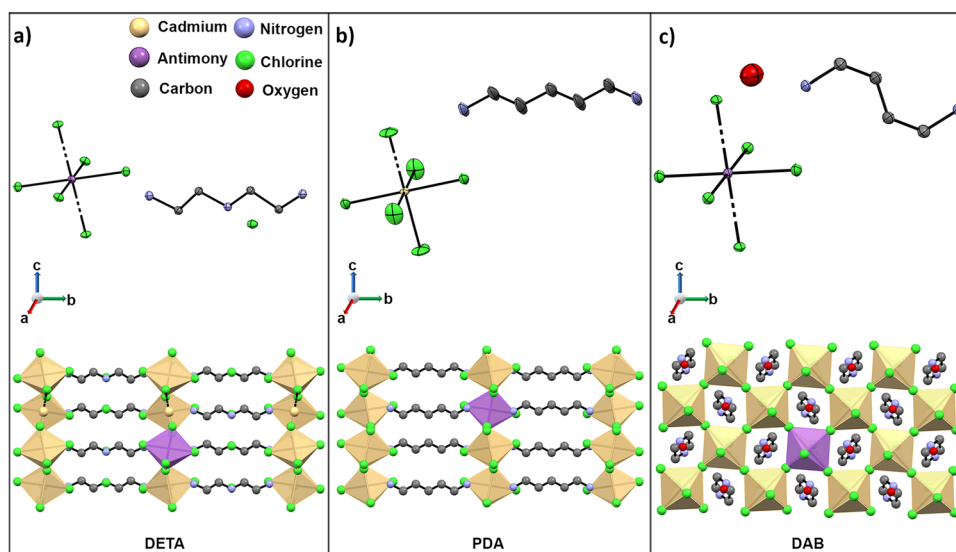

Fig. 1 Asymmetric unit and crystallographic atomic structure obtained from single crystal X-ray diffraction (ScXRD) analysis of (a) Sb:DETACdCl; (b) Sb:PDACdCl; (c) Sb:DABCdCl metal halide hybrids. Cadmium halide octahedra are highlighted with brown color and Sb-doped octahedra are highlighted with blue color. For clarity, H atoms have been omitted and unit cell axes (a, b, c) are shown for perspective in the packed structure.

This journal is © The Royal Society of Chemistry 2025

J. Mater. Chem. C, 2025, **13**, 808–820 | 811

details of the host and doped hybrids are provided in the ESI† (Tables S3 and S4) while Tables S5–S13 (ESI†) provide a summary of ScXRD structural analysis and tables of bond lengths, bond angles, and dihedral angles for all the compounds.

Briefly, the Sb:DETACdCl system crystallizes in the orthorhombic crystal system with *Pnma* space group, Sb:PDACdCl crystallizes in the orthorhombic crystal system with *Imma* space group, and Sb:DABCdCl crystallizes in the monoclinic system with $P2_1/c$ space group with water molecules present in the structure. This is in accordance with the structure of the corresponding host systems (Table S4, ESI†). The experimental powder X-ray diffraction (PXRD) patterns match well with the simulated one (Fig. S5 and S6, ESI†) confirming the phase purity of the synthesized host and doped hybrids. To note, the control hybrids have different structures as compared to the host and doped systems. DETASbCl crystallizes in the triclinic system ($P\bar{1}$ space group) forming a non-networked 0D assembly of highly distorted octahedral Sb–halide units dispersed in the cation matrix. PDASbCl forms a 1D structure with an orthorhombic crystal system ($P2_12_12_1$ space group) wherein a linear chain of corner shared Sb–halide octahedral units are charge balanced by the organic cation. DABSbCl crystallizes in the monoclinic system ($P2_1/c$ space group) with 0D rendition of the square pyramidal Sb–halide units. The simulated and experimental PXRD of the control systems are in agreement with each other indicating the phase purity of the control systems (Fig. S7–S9, ESI†).

Structural properties and distortions of host hybrids are presented in Table S2, ESI† while Table 1 provides the structural properties of the doped systems. The doped hybrids, all having a 2D DJ structure, show different extents of metal halide distortions/site symmetry due to their interactions with the organic cations. The metal halide distortions around the dopant centre are expected to have notable impact on their photophysical properties. Hence, we have calculated the following parameters for characterization of the structural distortions in Sb-doped 2D hybrids: (i) bond length distortions (octahedral elongation); (ii) bond angle variance; (iii) metal–halide–metal bond angles (M–Cl–M); and (iv) angle of tilt ($\phi_{tilt\,(deg)}$). A summary of the distortion parameters along with the photophysical properties is provided in Table 1 (doped hybrids) and Table S2 (ESI†) (host hybrids). The octahedral distortion is calculated based on the equation[33]

$$\Delta d = \frac{1}{6} \sum_{n=1}^{6} \left[\frac{d_n - d}{d} \right]^2$$

where Δd is the octahedral distortion, d_n represents the individual bond lengths, and d represents the average bond length.

The bond angle variance is calculated as per the equation[33]

$$\sigma^2 = \frac{1}{11} \sum_{n=1}^{12} [\theta_n - 90°]^2$$

where σ^2 is the bond angle variance and θ_n represents the Cl–Cd/Sb–Cl bond angle.

Sb:DETACdCl has lower distortion parameters: bond length distortion ($\Delta d = 9.04 \times 10^{-5}$), M–Cl–M (153.54°), bond angle variance ($\sigma^2 = 2.2432$) and tilt angle ($\phi_{tilt} = 11.26°$). The Sb:PDACdCl hybrid has distortion parameters: bond length distortion ($\Delta d = 1.5 \times 10^{-4}$), M–Cl–M (160.76°), bond angle variance ($\sigma^2 = 2.2300$) and tilt angle ($\phi_{tilt} = 12.45°$) showcasing comparatively higher distortions than the Sb:DETACdCl system. Furthermore, the Sb:DABCdCl system shows the highest degree of distortion: bond length distortion ($\Delta d = 1.4 \times 10^{-3}$), M–Cl–M (165.91°), bond angle variance ($\sigma^2 = 0.6409$) and tilt angle ($\phi_{tilt} = 13.02°$) likely due to the presence of the water molecules in the structure that can show strong hydrogen bonding interactions.[44] The structural distortion analysis clearly reveals the following trend in the extent of distortion-Sb:DABCdCl > Sb:PDACdCl > Sb:DETACdCl highlighting the strong impact of the choice of the organic amine on the local structure/distortion around the dopant centre in the doped 2D metal halide hybrids. A pictorial representation of the distortion parameters is shown in Fig. S10–S12; ESI.† Furthermore, by adjusting the feed percentage of the Sb precursor (relative to cadmium precursor) during the synthesis of the doped hybrids, the amount of incorporated dopants was varied systematically. The resulting percentage of Sb in the crystals, quantified *via* ICP analysis, is found to rise as the Sb feed percentage is increased (Table S1; ESI†). Furthermore, Fig. S13; ESI† shows a comparison between the PXRD patterns of the host and various percentages of Sb-doped samples. Notably, across all the doped systems, altering the dopant percentage did not induce any significant changes in the crystal structure as supported by the absence of peak shifts or the appearance of new peaks in the PXRD patterns of the doped samples. Encouragingly, variation of the Sb feed percentage for a given hybrid allowed maximizing the photoluminescence intensity. This results in the successful synthesis of Sb doped hybrids containing different organic cations with the highest emission strength. Hereafter, Sb-doped samples (with different organic cations) with the brightest emission were further characterized and analyzed for drawing structure–photophysical property correlations.

The impact of the extent of the structural distortions present in the Sb-doped metal halide hybrids is observable in their strikingly different luminescence properties, as summarized in Table 1. Unlike the non-luminescent host hybrids, the Sb doped

Table 1 Structural and optical properties of the synthesized Sb-doped 2D cadmium halide hybrids

Compound	Space group	Octahedral distortion (d)	Bond angle variance (deg²)	M–Cl–M (deg)	ϕ_{tilt} (deg)	PL Max (nm)	PLE peak positions (nm)	PLQY (%)
Sb:DETACdCl $C_4H_{16}N_3Cd\,Cl_5$	Orthorhombic *Pnma*	9.04×10^{-5}	2.2432	153.54	11.26	520	271, 290, 330	60
Sb:PDACdCl $C_5H_{16}N_2Cd\,Cl_4$	Orthorhombic *Imma*	1.5×10^{-4}	2.2300	160.76	12.45	540	281, 293, 333	61
Sb:DABCdCl $2(C_4H_{14}N_2)\,Cd_2Cl_8O$	Monoclinic $P2_1/c$	1.4×10^{-3}	0.6409	165.91	13.02	560	275, 291, 333	96

812 | *J. Mater. Chem. C*, 2025, **13**, 808–820

This journal is © The Royal Society of Chemistry 2025

hybrids show bright green/yellowish green/yellowish orange emission when viewed under UV excitation (365 nm), as shown in the insets of Fig. 2. The optical properties (absorbance, photoluminescence-PL, photoluminescence excitation-PLE) of the doped systems are shown in Fig. 2 while the peak positions of the PL and PLE spectra along with the photoluminescence quantum yield (PLQY) for the doped hybrids are listed in Table 1. The Sb:DETACdCl system shows a strong emission centered at 520 nm when excited at 272 nm with PLQY $\sim$ 60%. The PLE collected at 520 nm shows sharp onset around 375 nm characteristics of Sb doped hybrids confirming the successful incorporation of Sb in the hybrids. The PL and PLE profiles remain unchanged across the excitation and emission range, respectively (Fig. S14; ESI†). The Sb:PDACdCl system shows an emission peak at 540 nm when it is excited at 293 nm with a PLQY $\sim$ 61%. The PLE feature is comparable with that of the Sb:DETACdCl system. The PL and PLE profiles remain unaltered throughout the excitation and emission ranges (Fig. S15; ESI†). The Sb:DABCdCl system has an emission at 560 nm when excited at 274 nm with high PLQY $\sim$ 96%. The PLE features remain similar for all the systems with respect to the corresponding emissions (Fig. S16; ESI†). The absence of any additional excitation dependent emissive features for the Sb-doped hybrids strongly suggests that the observed emissions originate from unique emissive Sb^{3+} dopant species. Sb^{3+} dopant ions, with ns^2 configuration, have ground state $^1S_0$ and excited state $^1P_1$ and ^3P_n ($n = 0,1,2$). The transitions $^1S_0 \rightarrow \, ^3P_0$ and $^1S_0 \rightarrow \, ^3P_2$ are forbidden while $^1S_0 \rightarrow \, ^1P_1$ and $^1S_0 \rightarrow \, ^3P_1$ are partially allowed due to spin–orbit coupling (C and A band, respectively). The observed PLE features of the doped hybrids in the $\sim$ 280–290 nm region and $\sim$ 340–350 nm region correspond to C and A bands, respectively (Fig. 2). PL lifetime decay analysis of these Sb-doped hybrids provides long lived emissions with average lifetime values of 2.0 µs, 2.6 µs and 3.1 µs for Sb:DETACdCl, Sb:PDACdCl and Sb:DABCdCl hybrids, respectively (Fig. 2(d)). The observed long lifetimes with characteristic broad emission and PLE features for the Sb doped hybrids are in accordance with the generally accepted self-trapped excitonic (STE) emissive nature of the strongly luminescent Sb dopants in the doped hybrids. Optical characterization of the host and control systems, discussed below, further support the assignment of Sb^{3+} as the emissive species in the doped hybrids.

The host hybrids reported here are weakly emissive with low PLQY. The DETACdCl hybrid has a weak emission peak centered at 490 nm (PLQY $\sim$ 3.5%) with PLE peaks in the 270–290 nm and 330–350 nm regions (Fig. S17; ESI†). The PDACdCl hybrid shows a weak emission peak at 480 nm with PLQY $\sim$ 0.5%. The PLE collected at 480 nm has a narrow feature in the 400 nm region (Fig. S17; ESI†). The DABCdCl hybrid has PL peaks at 440 nm and 465 nm (PLQY $\sim$ 3.6%). The PLE shows features similar to that of the DETACdCl hybrid (Fig. S17; ESI†). The average lifetime values, estimated at 80 K, are 7.8 ns, 5.4 ns and 7.4 ns for the DETACdCl, PDACdCl, and DABCdCl hybrid hosts, respectively (Fig. S17; ESI†). Noteworthy here, the measured lifetimes of the doped systems are in the microsecond timescale, much longer than the host lifetimes (nanoseconds).
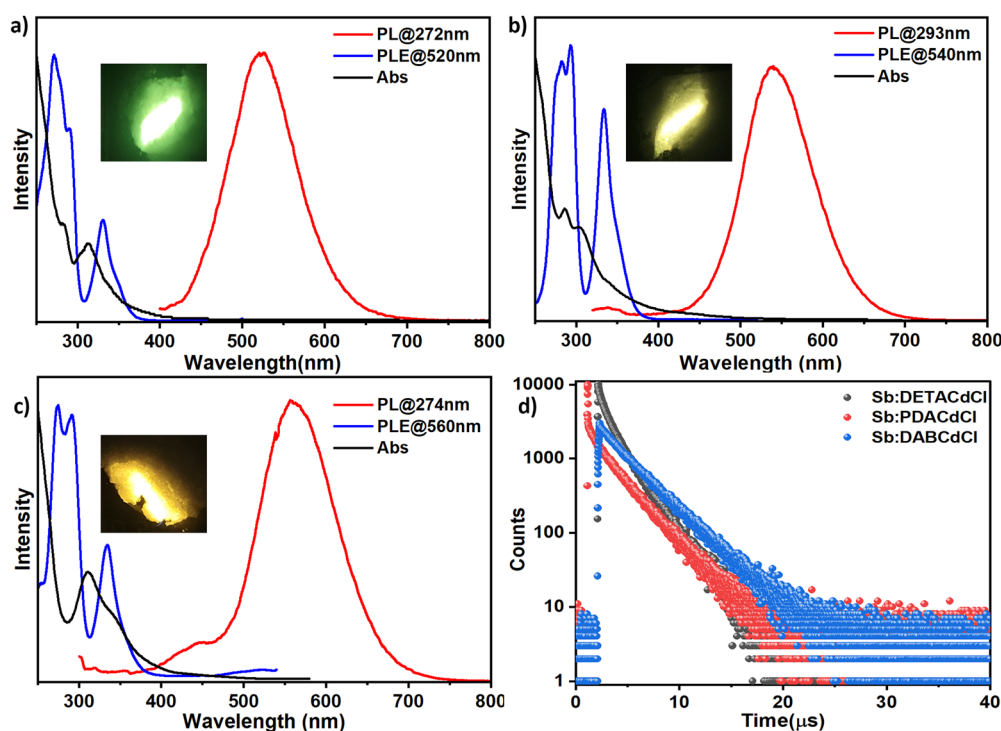

Fig. 2 Optical characterization of (a) Sb:DETACdCl, (b) Sb:PDACdCl, and (c) Sb:DABCdCl hybrids showing absorbance, photoluminescence and photoluminescence excitation spectra. (d) Lifetime decay profile of Sb:DETACdCl, Sb:PDACdCl and Sb:DABCdCl. The inset shows the photographs of the crystals when excited at 330 nm.

This journal is © The Royal Society of Chemistry 2025

J. Mater. Chem. C, 2025, **13**, 808–820 | **813**

The weak blue emission observed in the host hybrids likely arises due to emission contribution from both the organic cations and cadmium halide framework (Fig. S18; ESI†). Next, the optical properties of the control systems are presented in Fig. S19; ESI.† The DETASbCl hybrid emits weakly at 560 nm (PLQY ∼ 2%) when excited at 360 nm. The PLE exhibits characteristic Sb^{3+} absorption features with a sharp onset at 400 nm. The PDASbCl hybrid has a weak emission at 570 nm (PLQY ∼ 0.1%) while the DABSbCl hybrid has a PL peak centred at 560 nm (PLQY ∼ 1.8%) with PLE features comparable to that of the DETASbCl hybrids. The lifetime of the weak emissions of the control systems, measured at 80 K, were estimated to be in the microsecond timescales (DETASbCl ∼ 2.9 μs, PDASbCl ∼ 3.7 μs, and DABSbCl ∼ 3.9 μs). Notable here is the similarity of the lifetime values of the control and doped systems. Cumulatively, the comparative analysis of the optical properties of the doped, host, and control systems suggests that the luminescence in the doped 2D hybrids originates from the substitutional Sb^{3+} dopant centres.

Low temperature PL/PLE measurements were performed in the range of 80–300 K to get more insight towards the emission mechanism in the doped hybrids. From the measured temperature dependent PL (excited at 330 nm; Fig. 3(a)–(c)), it is observed that the doped systems show a monotonic trend of decreasing intensity of emission as the temperature is increased from 80 K to 300 K. This is due to the opening up of non-radiative channels as the temperature is raised thereby lowering the PL intensity. Fig. S20; ESI† shows the temperature dependent PL for other excitations and PLE for the corresponding emissions. Fig. 3(d)–(f) shows

the Huang–Rhys factor (S) for the doped systems. The S value usually indicates the strength of electron–phonon coupling in the soft/flexible metal halide hybrids. The Huang–Rhys factor (S) can be estimated as per the equation[33]

$$\text{FWHM} = 2.36\sqrt{S}\hbar\omega_{\text{phonon}}\sqrt{\coth\frac{\hbar\omega_{\text{phonon}}}{2K_{\text{B}}T}}$$

where T is the temperature (K), $\hbar\omega_{\text{phonon}}$ is the longitudinal optical phonon frequency and K_{B} is the Boltzmann constant. The Huang–Rhys factors, obtained by fitting the temperature dependent FWHM values to the above equation, are 15.9, 25.4 and 18.8 respectively for Sb:DETACdCl, Sb:PDACdCl, and Sb:DABCdCl hybrids. The estimated S values are high indicating the soft nature of the doped hybrids that allow strong electron–phonon coupling supporting self-trapped excitonic emission in the doped systems.

Comparison of the room temperature photophysical properties of the doped hybrids incorporating different organic cations clearly reveals differences in the emission peak positions and PLQY values (Table 1). The CIE coordinates for the doped samples are given in Fig. 4(c), which depicts the change in emission color for the doped samples as the local metal halide geometry asymmetry/distortion changes (Table 1). Local metal halide asymmetry along with other factors (crystallographic defects, impurities, surface) may be responsible for the observed changes in the luminescence behavior of the hybrids. However, the synthesis method is optimized to incorporate Sb^{3+} dopants that maximize PLQY without changing the photo-
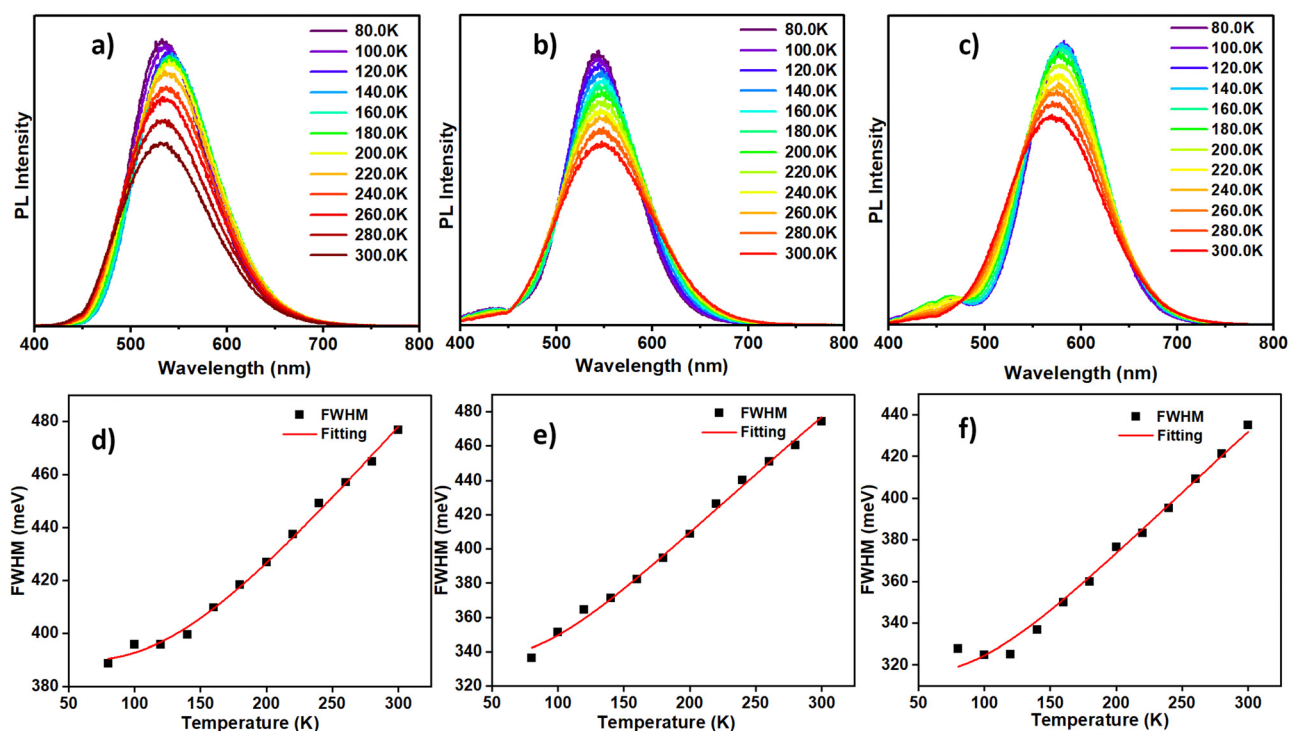

Fig. 3 (a)–(c) Temperature dependent emission spectra collected at ex: 330 nm [a – Sb:DETACdCl, b – Sb:PDACdCl, c – Sb:DABCdCl]; (d), (e) FWHM vs. temperature plot [d – Sb:DETACdCl, e – Sb:PDACdCl, f – Sb:DABCdCl].

814 | J. Mater. Chem. C, 2025, **13**, 808–820

This journal is © The Royal Society of Chemistry 2025

physical properties. Furthermore, the luminescence profiles do not vary from single crystals to powders for a given doped system (Fig. S21; ESI†). These observations suggest that local metal halide asymmetry may have a strong impact on the photo-physical properties of the hybrids. It is evident that the least distorted (octahedral elongation and bond angle distortion) doped system (Sb:DETACdCl) shows blue shifted emission (520 nm) while the highly distorted doped system (Sb:DABCdCl) shows red shifted emission (560 nm). The moderately distorted doped system (Sb:PDACdCl) has emission (540 nm) lying in between the Sb:DETACdCl and Sb:DABCdCl hybrids. Interestingly, the doped hybrids show different PLQY ranging from 60% to ∼96% correlated with the extent of distortion. The strongly distorted Sb:DABCdCl doped hybrid (incorporating water molecules in the crystal structure) showcases the highest PLQY when compared with the less distorted doped hybrids (Sb:PDACdCl; Sb:DETACdCl; Table 1). Overall, it is observed that the ground state distortion of the doped hybrids is correlated with the PL emission shifted to longer wavelengths and associated with higher PLQY.

Excitingly, it is found that the brightly emitting Sb:DABCdCl hybrid, incorporating water molecules in the crystal structure, shows a highly quenched emission when dehydrated, as shown in Fig. 5(a). The room temperature PLQY of the hydrated hybrid decreases from 96% to 39% when dehydrated. Heating the as prepared Sb:DABCdCl sample releases water molecules and shows an accompanying decrease in PL intensity (Fig. 5(b)) albeit maintaining similar PL/PLE/lifetime profiles (Fig. S22; ESI†). Such dehydrated Sb:DABCdCl hybrid was characterized using SCXRD and thermogravimetric analysis (TGA) confirming the absence of water molecules in the structure (Fig. S23; ESI†). Detailed distortion analysis of the dehydrated system reveals a comparable extent of distortion with that of the hydrated Sb:DABCdCl hybrid (Table S14; ESI†). However, the strong effect of the water molecule on the quenching of the luminescence intensity is clearly observed in the Sb:DABCdCl hybrid. A detailed understanding of the structural distortion parameters (modulated by the water molecule) and the luminescence properties is thus required to unravel the operative structure–luminescence relationship.

To better understand the electronic structure of the doped systems, density functional theory (DFT) calculations have been carried out. In all three systems (Sb:DETACdCl, Sb:PDACdCl,
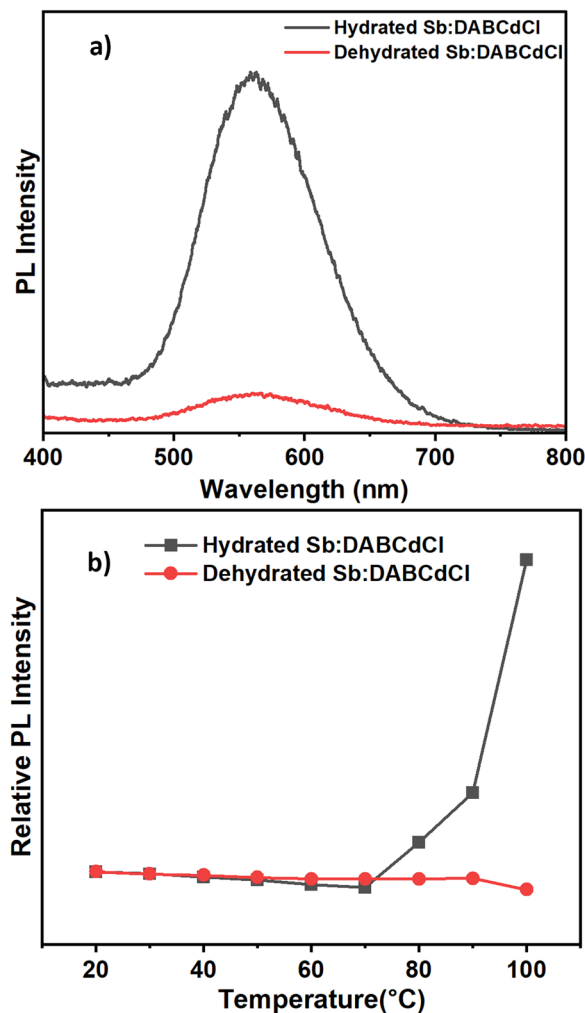

Fig. 5 (a) Comparison of the room temperature PL spectra of hydrated and dehydrated Sb:DABCdCl hybrids; (b) comparison of the temperature-dependent PL intensity (normalized) of hydrated and dehydrated Sb:DABCdCl hybrids.

and Sb:DABCdCl), 12.5% Sb-doping concentration has been considered, mimicking the 10% doped concentration observed experimentally from the ICP analysis. The projected density of states (DOS), as indicated in Fig. 6 shows that Sb:DABCdCl has the highest electronic band gap of 3.84 eV, whereas the
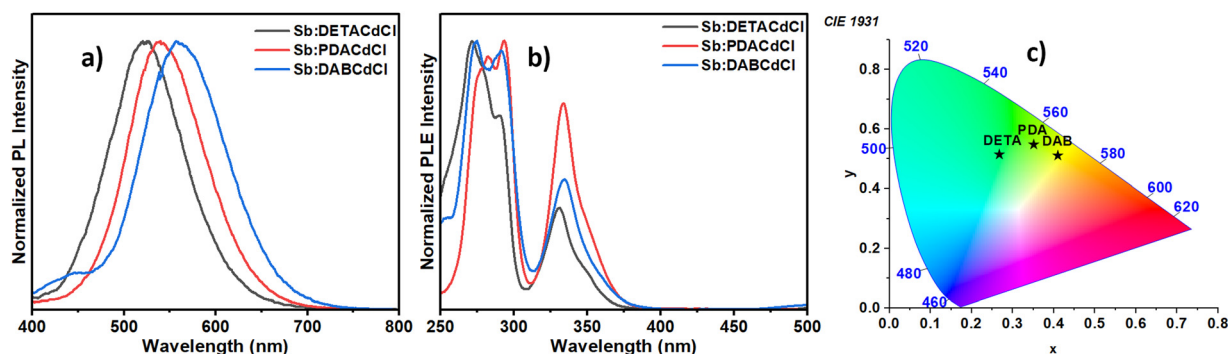

Fig. 4 Comparison of the (a) PL spectra; (b) PLE spectra; and (c) CIE chromaticity coordinates (CIE 1931) of Sb:DETACdCl, Sb:PDACdCl and Sb:DABCdCl hybrids.

This journal is © The Royal Society of Chemistry 2025

J. Mater. Chem. C, 2025, **13**, 808–820 | **815**

Sb:DETACdCl and Sb:PDACdCl structures have the band gap of 3.62 and 3.19 eV, respectively. These band gap values align well with the experimental band gap trend of 3.43, 3.39, and 3.30 eV for the Sb:DABCdCl, Sb:DETACdCl and Sb:PDACdCl systems, respectively (shown in Fig. S24; ESI†). The higher absolute values of the band gap may be due to the lack of inclusion of the excitonic effect in the structures, which may significantly reduce the values in lower dimensions. However, the use of the hybrid function in conjunction with the spin–orbit coupling reliably captures trends in the band gap and accurately describes the positions of the band edges, as has been routinely done by some of us.[45,46] Analysis of the DOS (Fig. 6) and the band edge charge density localization (Fig. S25; ESI†) of all three structures suggest that the Sb-center, along with the Cd-center, is populated at both the VBM and CBM, which indicates that the Sb-center can act as the luminescence source. Furthermore, in the case of Sb:DABCdCl, the H_2O molecule in the crystal structure also appears in the VBM and CBM indicating that it may play a role in the luminescence behavior. To understand the bandgap reduction from Sb:DABCdCl to Sb:PDACdCl, we have aligned the DOS of the three systems with respect to the deepest energy level of α-carbon.[47,48] Our results find that, while moving from Sb:DABCdCl to Sb:DETACdCl, both the VBM and CBM downshifted in energy by 0.17 and 0.39 eV, respectively with an overall band gap reduction of 0.22 eV. On the other hand, the VBM is upshifted by 0.22 eV and the CBM is downshifted by 0.43 eV, thus revealing a significant bandgap reduction of 0.65 eV in Sb:PDACdCl, compared to that of Sb:DABCdCl. Furthermore, the calculated band structure (PBE + SOC level of theory; Fig. S26; ESI†) shows the indirect nature of the bands, thus indicating higher carrier lifetime of the doped systems.

Experimentally, it has been observed that the formation of STE in the doped (Sb^{3+}) center results in dopant-based Sb emission, resembling the 0D Sb halide hybrids, with minimal contribution from the host emission across all structures. However, the PLQY of the studied structures ranges from approximately 60% to 96%, indicating a unique structure–luminescence relationship. To understand the STE formation and its role in the PLQY, we have investigated the excited state behavior by modelling the triplet configuration of all three structures. The excited state DOS (Fig. 7(a)–(c)) reveals that the Sb^{3+} center is predominantly concentrated at the band edges, along with some contribution from Cd and the organic ligands in all the three structures. However, in the case of Sb:DABCdCl, the H_2O molecule of the system appears at the band edges, thus acting as an efficient emission channel, resulting in an increased luminescence with a higher PLQY compared to that of Sb:PDACdCl and Sb:DETACdCl. For further quantification, the excited state electron and hole localization have been plotted (Fig. 7(f)–(h)) and the spatial overlap between the electron and hole wave functions has been considered as the extent of STE confinement. We have defined the electron and hole spatial overlap by calculating the percentage of volume occupied by the STE charge density with respect to the total volume of charge density; thus, a higher overlap percentage
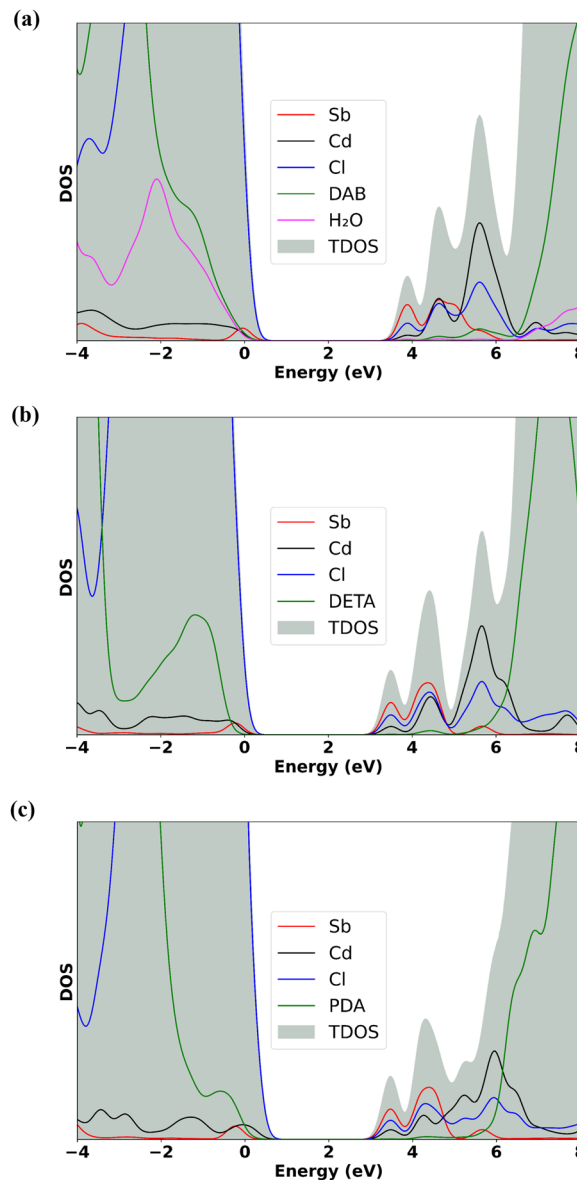

Fig. 6 Projected density of states (HSE06-SOC level) of (a) Sb:DABCdCl, (b) Sb:DETACdCl and (c) Sb:PDACdCl. In the DOS plots, the VBM of Sb:DABCdCl has been set to zero and aligned with the deepest energy level of α-carbon.

indicates a more confined STE. As can be seen from Fig. 7 and Table 2, the STE is localized at the inorganic (Sb^{3+}, Cd^{2+}) center and disperses into the organic moiety in the case of Sb:DETACdCl and Sb:PDACdCl with an electron/hole spatial overlap of 26.4 and 26.49%, respectively. Interestingly, in the case of Sb:DABCdCl, the electron and hole charge density are localized at the inorganic unit and water molecule with the electron/hole overlap of 34.04%, thus indicating the more confined STE compared to that of Sb:DETACdCl and Sb:PDACdCl. Therefore, the more localized STE leads to a higher PLQY in the case of Sb:DABCdCl.

Upon photoexcitation, the contraction of the SbCl and CdCl octahedra facilitates the stabilization of the trapped holes by forming self-trapped charged states. Therefore, a photo-
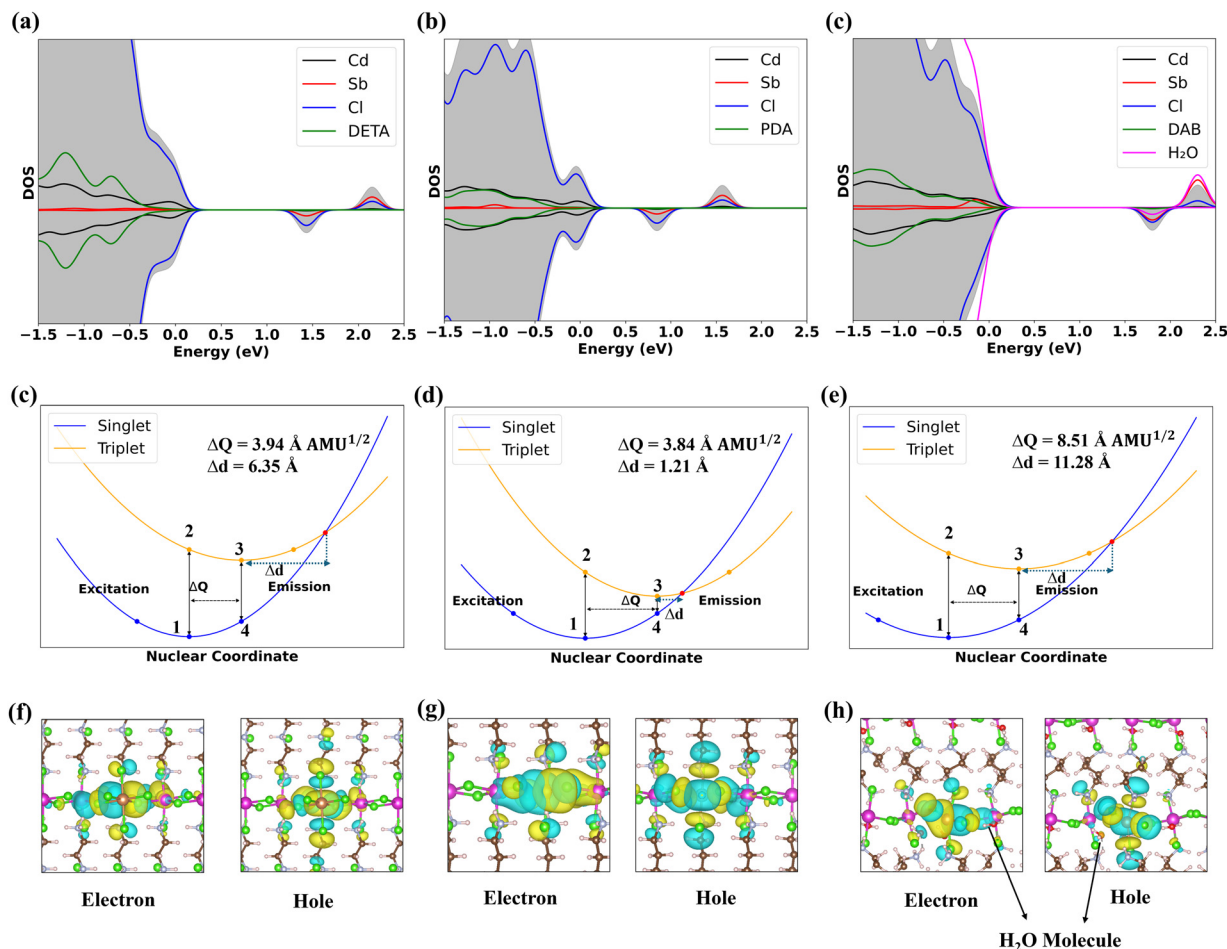
Fig. 7 (a)–(c) The excited state DOS with the triplet configuration; (c)–(e) the configuration coordinate diagram and (f)–(h) the zoomed-in figure of Kohn–Sham (KS) orbitals of the electron and hole in the STE state for Sb:DETACdCl, Sb:PDACdCl and Sb:DABCdCl, respectively.

generated hole tends to be self-trapped in an octahedron, eventually distorting the surrounding electron cloud *via* coulombic attraction to form the STE.[44,49] To quantify the octahedral contraction phenomena, we have calculated the Sb–Cl bond length contraction upon photoexcitation. In the case of Sb:DETACdCl and Sb:PDACdCl, the average Sb–Cl bond length contractions are 3.85 and 4.15%, respectively, which are lower compared to that of 5.98% in the case of Sb:DABCdCl, thus indicating the most confined STE formation in Sb:DABCdCl, matching with our charge density localization trend. Enhanced lattice distortion at the excited state leads to strong electron–phonon (e–ph) interaction[50] in the system, leading to more STE formation. To quantify such lattice distortion, we have calculated the ΔQ (mass-weighted displacement) between the atomic geometries of the ground state (GS) and the excited state (ES), which has a linear correlation with the electron–phonon coupling constant as:

$$\Delta Q = \left[\sum_{\alpha=1}^{N_{atom}} \sum_{i=x,y,z} M_\alpha \left(R_{\alpha i}^{ES} - R_{\alpha i}^{GS} \right)^2 \right]^{\frac{1}{2}}$$

where M_α is the mass of the αth atom, and $R_{\alpha i}^{GS}$ ($R_{\alpha i}^{ES}$) is the atomic coordinate of the αth atom in the ith direction of the

Table 2 Mass-weighted displacements (ΔQ), nuclear shift of the cross over point from the STE state (Δd), and the percentage of volume occupied by electrons and holes at the excited state values for the three systems

	ΔQ			
	All atoms (Å AMU$^{1/2}$)	All inorganic unit (Å AMU$^{1/2}$)	Δd (Å)	Electron hole overlap (%)
Sb:DETACdCl	3.95	3.92	6.35	26.42
Sb:PDACdCl	3.48	3.46	1.21	26.49
Sb:DABCdCl (hydrated)	8.51	8.00	11.28	34.04
Sb:DABCdCl (dehydrated)	5.30	4.96	6.66	25.41

GS (ES). The higher ΔQ value of Sb:DABCdCl indicates higher e–ph interaction and hence efficient STE-based emission compared to that of Sb:DETACdCl and Sb:PDACdCl. Such higher ΔQ in Sb:DABCdCl can be attributed to the presence of eight water molecules in the crystal, which form hydrogen bonds with the nitrogen atoms of the organic DAB cations, making the organic cation effectively larger in size and causing a higher extent of distortion in the bond lengths and bond angles.[44]
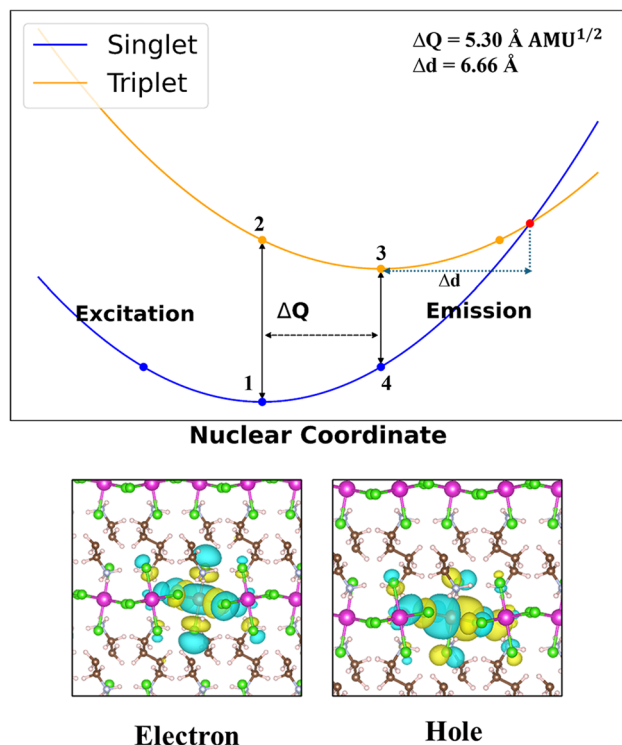
Fig. 8 Configuration coordinate diagram of dehydrated Sb:DABCdCl (upper panel) and the bottom panel represents the zoomed-in figure of Kohn–Sham (KS) orbitals of the electron and hole in the STE state.

Furthermore, we have plotted the configuration coordinate diagram (CCD) of the ground and excited state of all three systems as presented in Fig. 7(c)–(e), where points 1 and 3 define the singlet ground state geometry and triplet excited state geometry (STE state), respectively. As described in the configuration coordinate diagram, ΔQ is the mass-weighted displacement as shown above, and Δd is the cross-over distance, *i.e.*, the nuclear coordinate shift from the STE state to the singlet/triplet crossover point. The values are shown in Table 2. As can be seen from Fig. 7, the Δd values are 6.35 and 1.21 Å for Sb:PDACdCl and Sb:DETACdCl, respectively whereas, it is the highest with the value of 11.28 Å in the case of Sb:DABCdCl. A higher Δd indicates a greater nuclear coordinate shift from the STE state to the crossover point, which suggests that more electron–phonon interaction is required to meet the crossover point, thereby reducing the possibility of crossover. Consequently, such a low crossover possibility can reduce the non-radiative loss, eventually leading to a higher PLQY in the case of Sb:DABCdCl.

To check the role of H_2O molecules as an emission channel, we have done the excited state calculation for the crystal structure of the dehydrated Sb:DABCdCl hybrid (Fig. 8). Interestingly, we have found that the ΔQ value significantly decreases from 8.00 Å in the hydrated structure to 5.30 Å in the dehydrated one, indicating a substantial reduction in structural distortion upon photoexcitation. Additionally, the octahedral contraction also decreases from 5.98 to 3.90%. The spatial overlap between electrons and holes decreases from 34.04% to 25.41%, suggesting a notable reduction in STE confinement. The CCD diagram (Fig. 8) for the dehydrated

sample also shows a decrease in the Δd value to 6.66 Å compared to that of the 11.28 Å in the hydrated sample. The reduction in structural distortion, octahedral contraction, electron–hole overlap, and Δd value suggests that the absence of water molecules in the crystal plays a significant role in reducing the extent of STE formation and hence in the reduction of PLQY, thus nicely correlating with the observed experimental trend.

The theoretical insights gained herein allow us to conclude that the higher distortion indices (octahedral contraction, ΔQ, Δd) and confined STE formation lead to a higher PLQY value in the case of Sb:DABCdCl compared to that of Sb:PDACdCl and the Sb:DETACdCl hybrid in line with the experimental observations.

Conclusion

Reported here is a combined experimental–computational approach to unravel the operative structure–property correlation in Sb^{3+}-doped 2D cadmium halide hybrids. Rational choice of the organic cation controls the local metal halide geometry/asymmetry in the cadmium halide host hybrids that act as a framework to introduce Sb^{3+} dopants with tunable local distortions (octahedral distortion and bond angle variance estimated through single crystal XRD). The impact of the extent of the metal halide distortions on their photo-physical properties is strongly manifested in the form of a clear structure property correlation: red-shifted emission peak positions and enhanced photoluminescence quantum yields as the extent of the local metal halide distortion increases. DFT calculations validate the experimental findings on emission wavelengths and the formation of stable STEs in Sb-doped structures, crediting higher distortion indices and confined STE formation as a reason for higher PLQY. Furthermore, this work highlights the critical role of the H_2O molecules in the Sb:DABCdCl structure, revealing that the H_2O molecule not only causes structural distortion but also serves as an efficient emission channel. This work highlights the success of synthetic control in unravelling the structure–luminescence relationship in Sb^{3+} doped 2D cadmium halide hybrids and provides deeper insight into their observed photo-physical properties (PL peak position; PLQYs) showcasing the importance of ground and excited state structural distortions. Such insight is beneficial for drawing structure–property relationships for 0D Sb halide hybrids enabling their rational design and targeted synthesis for next generation luminescent materials.

Data availability

The data supporting this article have been included as part of the ESI.† Supplementary Information: EDS data, PL/PLE characterization, PXRD data, SCXRD data of bond lengths and bond angles; crystallographic data for DETACDCl, Sb:DETACdCl, DETASbCl, PDACdCl, Sb:PDACdCl, PDASbCl, DABCdCl, Sb:DABCdCl, DABSbCl, and SB:DABCdCl (Dehydrated) has been deposited at the CCDC under 2376168, 2376167, 2376166, 2376174, 2376169, 2376170, 2376173, 2376171, 2376172, and 2376179.

818 | *J. Mater. Chem. C*, 2025, **13**, 808–820

This journal is © The Royal Society of Chemistry 2025

Conflicts of interest

The authors declare no competing financial interest.

Acknowledgements

References

1 L. Mao, J. Chen, P. Vishnoi and A. K. Cheetham, *Acc. Mater. Res.*, 2022, **3**, 439–448.

2 M. Li and Z. Xia, *Chem. Soc. Rev.*, 2021, **50**, 2626–2662.

3 C. Zhou, L.-J. Xu, S. Lee, H. Lin and B. Ma, *Adv. Opt. Mater.*, 2021, **9**(18), 2001766.

4 L. Zhou, J.-F. Liao and D.-B. Kuang, *Adv. Opt. Mater.*, 2021, **9**, 2100544.

5 J.-S. Yao, J.-J. Wang, J.-N. Yang and H.-B. Yao, *Acc. Chem. Res.*, 2021, **54**, 441–451.

6 J. Kundu and D. K. Das, *Eur. J. Inorg. Chem.*, 2021, 4508–4520.

7 C. Katan, N. Mercier and J. Even, *Chem. Rev.*, 2019, **119**, 3140–3192.

8 H. Peng and B. Zou, *J. Phys. Chem. Lett.*, 2022, **13**, 1752–1764.

9 Z. Song, J. Zhao and Q. Liu, *Inorg. Chem. Front.*, 2019, **6**, 2969–3011.

10 K. Leng, W. Fu, Y. Liu, M. Chhowalla and K. P. Loh, *Nat. Rev. Mater.*, 2020, **5**, 482–500.

11 L. Mao, C. C. Stoumpos and M. G. Kanatzidis, *J. Am. Chem. Soc.*, 2018, **141**, 1171–1190.

12 C. Huo, B. Cai, Z. Yuan, B. Ma and H. Zeng, *Small Methods*, 2017, **1**, 1600018.

13 C. Zhou, H. Lin, S. Lee, M. Chaaban and B. Ma, *Mater. Res. Lett.*, 2018, **6**, 552–569.

14 Z. Gan, Y. Cheng, W. Chen, K. P. Loh, B. Jia and X. Wen, *Adv. Sci.*, 2021, **8**, 2001843.

15 D. B. Straus and C. R. Kagan, *Annu. Rev. Phys. Chem.*, 2022, **73**, 403–428.

16 K. Han, J. Jin, B. Su and Z. Xia, *Trends Chem.*, 2022, **4**, 1034–1044.

17 M. Z. Rahaman, S. Ge, C.-H. Lin, Y. Cui and T. Wu, *Small Struct.*, 2021, **2**, 2000062.

18 J.-C. Blancon, J. Even, C. C. Stoumpos, M. G. Kanatzidis and A. D. Mohite, *Nat. Nanotechnol.*, 2020, **15**, 969–985.

19 C. M. Mauck and W. A. Tisdale, *Trends Chem.*, 2019, **1**, 380–393.

20 Z. Li, Y. Li, P. Liang, T. Zhou, L. Wang and R.-J. Xie, *Chem. Mater.*, 2019, **31**, 9363–9371.

21 C. Sun, Z. Deng, Z. Li, Z. Chen, X. Zhang, J. Chen, H. Lu, P. Canepa, R. Chen and L. Mao, *Angew. Chem., Int. Ed.*, 2023, **62**, e202216720.

22 V. Morad, S. Yakunin and M. V. Kovalenko, *ACS Mater. Lett.*, 2020, **2**, 845–852.

23 L. Mao, P. Guo, S. Wang, A. K. Cheetham and R. Seshadri, *J. Am. Chem. Soc.*, 2020, **142**, 13582–13589.

24 V. Morad, I. Cherniukh;, P. Lena, S. Yevhen, Y. Sergii and M. V. Kovalenko, *Chem. Mater.*, 2019, **31**, 10161–10169.

25 Y.-Y. Ma, H.-Q. Fu, X.-L. Liu, Y.-M. Sun, Q.-Q. Zhong, W.-J. Xu, X.-W. Lei, G.-D. Liu and C.-Y. Yue, *Inorg. Chem.*, 2022, **61**, 8977–8981.

26 K. M. McCall, V. Morad, B. M. Benin and M. V. Kovalenko, *ACS Mater. Lett.*, 2020, **2**, 1218–1232.

27 A. Biswas, R. Bakthavatsalam, B. P. Mali, V. Bahadur, C. Biswas, S. S. K. Raavi, R. G. Gonnade and J. Kundu, *J. Mater. Chem. C*, 2021, **9**, 348–358.

28 D.-Y. Li, J.-H. Song, Z.-Y. Xu, Y.-J. Gao, X. Yin, Y.-H. Hou, L.-J. Feng, C.-Y. Yue, H. Fei and X.-W. Lei, *Chem. Mater.*, 2022, **34**, 6985–6995.

29 J.-Q. Zhao, M.-F. Han, X.-J. Zhao, Y.-Y. Ma, C.-Q. Jing, H.-M. Pan, D.-Y. Li, C.-Y. Yue and X.-W. Lei, *Adv. Opt. Mater.*, 2021, **9**, 2100556.

30 C. Deng, S. Hao, K. Liu, M. S. Molokeev, C. Wolverton, L. Fan, G. Zhou, D. Chen, J. Zhao and Q. Liu, *J. Mater. Chem. C*, 2021, **9**, 15942–15948.

31 X. Zhang, L. Li, Z. Sun and J. Luo, *Chem. Soc. Rev.*, 2019, **48**, 517–539.

32 J. Nie, X. Yun, F. Cheng, B. Lan, R. Cao and J. Wang, *J. Mater. Chem. C*, 2024, **12**, 2571.

33 L.-K. Wu, R.-F. Li, W.-Y. Wen, Q.-H. Zou, H.-Y. Ye and J.-R. Li, *Inorg. Chem. Front.*, 2023, **10**, 3297–3306.

34 J. Lin, Z. Guo, N. Sun, K. Liu, X. Chen, J. Zhao, Q. Liu and W. Yuan, *J. Mater. Chem. C*, 2022, **10**, 5905–5913.

35 G. Zhang, C. Yang, Q. Wei, J. Long, X. Shen, Y. Chen, B. Ke, W. Liang, X. Zhong and B. Zou, *ACS Appl. Mater. Interfaces*, 2024, **16**, 3841–3852.

36 D. Zhu, M. L. Zaffalon, J. Zito, F. Cova, F. Meinardi, L. D. Trizio, I. Infante, S. Brovelli and L. Manna, *ACS Energy Lett.*, 2021, **6**, 2283–2292.

37 R. D. Shannon, *Acta Crystallogr.*, 1976, **A32**, 751–767.

38 P. Giannozzi, S. Baroni, N. Bonini, M. Calandra, R. Car, C. Cavazzoni, D. Ceresoli, G. L. Chiarotti, M. Cococcioni, I. Dabo, A. D. Corso, S. de Gironcoli, S. Fabris, G. Fratesi, R. Gebauer, U. Gerstmann, C. Gougoussis, A. Kokalj, M. Lazzeri, L. Martin-Samos, N. Marzari, F. Mauri, R. Mazzarello, S. Paolini, A. Pasquarello, L. Paulatto, C. Sbraccia, S. Scandolo, G. Sclauzero, A. P. Seitsonen, A. Smogunov, P. Umari and R. M. Wentzcovitch, *J. Phys.: Condens. Matter*, 2009, **21**, 395502.

39 S. Grimme, J. Antony, S. Ehrlich and H. Krieg, *J. Chem. Phys.*, 2010, **132**, 154104.

40 J. P. Perdew, K. Burke and M. Ernzerhof, *Phys. Rev. Lett.*, 1996, **77**, 3865–3868.

41 J. Heyd, G. E. Scuseria and M. Ernzerhof, *J. Chem. Phys.*, 2003, **118**, 8207–8215.

This journal is © The Royal Society of Chemistry 2025

J. Mater. Chem. C, 2025, **13**, 808–820 | 819

42 J. VandeVondele, M. Krack, F. Mohamed, M. Parrinello, T. Chassaing and J. Hutter, *Comput. Phys. Commun.*, 2005, **167**, 103–128.

43 M. Guidon, J. Hutter and J. VandeVondele, *J. Chem. Theory Comput.*, 2010, **6**, 2348–2364.

44 J.-B. Luo, J.-H. Wei, Z.-Z. Zhang and D.-B. Kuang, *Inorg. Chem.*, 2021, **61**, 338–345.

45 R. Das, M. Hossain, A. Mahata, D. Swain, F. De Angelis, P. K. Santra and D. D. Sarma, *ACS Mater. Lett.*, 2023, **5**, 1556–1564.

46 R. Chiara, M. Morana, M. Boiocchi, M. Coduri, M. Striccoli, F. Fracassi, A. Listorti, A. Mahata, P. Quadrelli, M. Gaboardi, C. Milanese, L. Bindi, F. De Angelis and L. Malavasi, *J. Mater. Chem. C*, 2021, **9**, 9899–9906.

47 M. Coduri, T. B. Shiell, T. A. Strobel, A. Mahata, F. Cova, E. Mosconi, F. De Angelis and L. Malavasi, *Mater. Adv.*, 2020, **1**, 2840–2845.

48 R. Das, D. Swain, A. Mahata, D. Prajapat, S. K. Upadhyay, S. Saikia, V. R. Reddy, F. De Angelis and D. Sarma, *Chem. Mater.*, 2024, **36**, 1891–1898.

49 C. Coccia, M. Morana, A. Mahata, W. Kaiser, M. Moroni, B. Albini, P. Galinetto, G. Folpini, C. Milanese and A. Porta, *Angew. Chem., Int. Ed.*, 2024, **63**, e202318557.

50 A. Mahata, E. Mosconi, D. Meggiolaro, S. Fantacci and F. De Angelis, *Adv. Energy Mater.*, 2023, 2303405.

820 | *J. Mater. Chem. C*, 2025, **13**, 808–820

This journal is © The Royal Society of Chemistry 2025